Delft University of Technology

Identification of internal damages in reinforced concrete slabs using probability density field of acoustic emission events

Zhang, F.; Yang, Y.; Hendriks, M.A.N.

Important note
To cite this publication, please use the final published version (if applicable).
Please check the document version above.

IDENTIFICATION OF INTERNAL DAMAGES IN REINFORCED CONCRETE SLABS USING PROBABILITY DENSITY FIELD OF ACOUSTIC EMISSION EVENTS

Fengqiao Zhang[1,*], Yuguang Yang[1] and Max A.N. Hendriks[1,2]

[1]Department of Engineering Structures, Delft University of Technology, Delft, the Netherlands;
F.Zhang-5@tudelft.nl, yuguang.yang@tudelft.nl, M.A.N.Hendriks@tudelft.nl
[2]Department of Structural Engineering, Norwegian University of Science and Technology, Trondheim, Norway
*Correspondence: F.Zhang-5@tudelft.nl

ABSTRACT

To assess the structural capacity of reinforced concrete structures, identifying the internal cracks is important. Acoustic emission (AE) is promising to estimate the location of internal cracks. However, the localization is influenced by many factors like arrival time picking error, presence of crack, etc., resulting in localization error. The error cannot be entirely removed. Considering the inevitable localization error, a probabilistic method was recently developed by the authors. The method estimates the probability of the location of AE events, creating a probability density field of AE events (pdAE field). This method can possibly improve the identification of internal damages. This paper evaluates the performance the pdAE field in identifying internal damages in a reinforced concrete slab. The slab was loaded to failure by a point load. Compared to the conventional localization results, the pdAE field showed a clearer internal crack pattern. Moreover, calculation of the pdAE field was time efficient, thus was suitable for real-time monitoring. With these benefits, the pdAE field indicated the failure of the slab before it occurred.

Keywords: Acoustic emission source localization, probability density field, damage identification, internal damages, reinforced concrete structures.

1. Introduction

To assess the structural capacity of reinforced concrete structures, identification of the location and magnitude of the internal cracks is important. Most techniques only measure the cracks on the structural surfaces, losing the information of the internal damages. A promising technique to detect the internal damages is acoustic emission (AE). Concrete changes like cracking will release energy and generate elastic waves, which propagate to the structural surface and are detected by the AE sensors. By analysing the received signals, AE can estimate the source location (which is source localization) [1], classify the source type (which is source classification) [2] and estimate the structural damage level [3]. Among all its capabilities, the scope of this paper is within source localization.

The conventional source localization methods strive to accurately locate AE sources. However, the localization accuracy is influenced by many factors, such as arrival time picking error,

uncertainty of concrete material properties, sensor locations, etc. These uncertainties cannot be entirely removed from the localization process.

A simplified probabilistic method was developed by the authors in a previous paper [4]. Instead of aiming to accurately locate the source, the probabilistic method quantifies the uncertainties in the localization process and estimates the probability of source location. For a given AE event obtained by a localization process, the method calculates the probability of the location of the event in the 1D, 2D or 3D space, which is called probability density field of the AE event (pdAE field). The probability density field of multiple AE events is obtained by adding up the field of each event. The pdAE field method can possibly improve the identification of the internal damages.

This paper aims to evaluate the performance of the pdAE field method in identifying the internal damages in reinforced concrete slabs. A reinforced concrete slab was loaded to failure by a point load. During load testing, we calculated the pdAE field of AE events in 3D. Compared to the estimated source locations from a traditional localization process, pdAE field shows a clearer internal crack distribution. Moreover, the calculation of pdAE field is time efficient, thus suitable for real-time monitoring. With clearer and real-time identification of internal cracks, the pdAE field is able to indicate the structural failure before it occurs.

2. Probability density field of acoustic emission events

The concept of the pdAE field method is to calculate the probability of the location of AE events based on the estimated source location which contains localization error. Two important inputs are the estimated source locations and the error properties.

The source location is estimated by deterministic localization methods such as grid search method [5] or more advanced method concerning a variable velocity distribution [6]. In principle, one can use any method but the corresponding error properties may differ. To evaluate the error properties, one can refer to a previous paper by the authors which provided a method based on simulations and validated by experiments [7].

The source localization error is defined as the relative location of the estimated source location to the actual location:

$$\mathbf{\Delta} = \mathbf{x_s} - \mathbf{x_g} \tag{1}$$

where, $\mathbf{x_s}$ is the actual source location and $\mathbf{x_g}$ is the estimated source location.

The magnitude of source localization error $\|\mathbf{\Delta}\|$ is the Euclidian distance between the actual and estimated source locations:

$$\|\mathbf{\Delta}\| = \sqrt{\sum_{i=1}^{k} \Delta_i^2} \, , k \in \{1,2,3\} \tag{2}$$

where, k is the dimension of the measuring zone which could be 1D, 2D or 3D and Δ_i is the error component in the ith direction.

The error component Δ_i is assumed following a normal distribution, with zero mean and standard deviation σ, which is the same for all directions. Then the probabilistic density function of the source localization error $\mathbf{\Delta}=(\Delta_1,\cdots,\Delta_k)^{\text{T}}$ is:

$$f(\mathbf{\Delta}) = \frac{1}{\left(\sqrt{2\pi}\right)^k} \frac{1}{\sigma^k} e^{-\|\mathbf{\Delta}\|^2/2\sigma^2} , k \in \{1,2,3\} \tag{3}$$

For 1D source localization, the scalar-valued error $\mathbf{\Delta}=\varDelta_1$ follows a normal distribution with mean zero and standard deviation σ. For 2D and 3D source localization, the error $\mathbf{\Delta}$ follows a multivariate normal distribution with uncorrelated error components $\varDelta_i$, with mean zero and the same standard deviation σ.

With the estimated source location as the origin, we are able to calculate the probability density at any point $\mathbf{x}$ as:

$$f(\mathbf{x}, \mathbf{x_g}) = \frac{1}{(\sqrt{2\pi})^k} \frac{1}{\sigma^k} e^{-\|\mathbf{x}-\mathbf{x_g}\|^2/2\sigma^2}, k \in \{1,2,3\} \tag{4}$$

where, $\mathbf{x_g}$ is the estimated source location, $\mathbf{x}$ is a random point in the space of k dimensions. The probability density $f(\mathbf{x},\mathbf{x_g})$ evaluates the likelihood that an AE event which is estimated at point $\mathbf{x_g}$ (from deterministic localization method) but is actually located at point $\mathbf{x}$. The probability density at points in the whole space create the probability density field of the AE event (pdAE field). The integration of probability densities over the whole space equals 1. Fig. 1a shows the pdAE field of an AE event that is estimated at location $\mathbf{S}$, when $k=2$ and $\sigma=39$ mm (the value of σ is taken from a previous simulated case [4]). The likelihood of the AE event located at p_1 is larger than that at p_2.

Regarding the source localization error magnitude $\|\mathbf{\Delta}\|$, since we assume that the error component follows a normal distribution, by definition, the error magnitude can be described by a chi distribution [8]:

$$g(\|\mathbf{\Delta}\|, k) = \frac{\|\mathbf{\Delta}\|^{k-1} e^{-\|\mathbf{\Delta}\|^2/(2\sigma^2)}}{2^{k/2-1}\Gamma(k/2)} \frac{1}{\sigma^k}, k \in \{1,2,3\} \tag{5}$$

For 1D source localization, $k=1$, the chi distribution is also known as half-normal distribution; for 2D source localization, $k=2$ leads to a Rayleigh distribution; for 3D source localization, the chi distribution with $k=3$ is Maxwell-Boltzmann distribution. Fig. 1b shows the three distributions when $\sigma=39$ mm. A higher degree of freedom k gives a larger expected value of error magnitude.
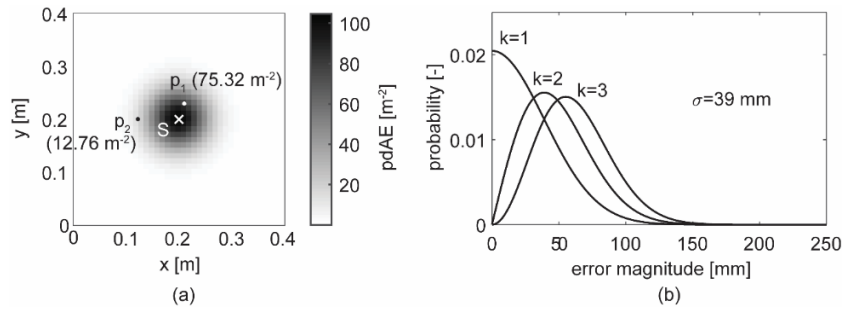

Fig. 1: Probability distribution of (a) the location of the source that is estimated at $\mathbf{S}$ (when $k=2$, $\sigma=39$ mm) and (b) the error magnitude (when $k=\{1,2,3\}$, $\sigma=39$ mm).

When more AE events occur during monitoring, the probability density field of each event is added, resulting in a probability density field of multiple AE events. For all AE events that occur in the measuring time and space range, the probability density at a random location $\mathbf{x}$ is calculated as:

$$p_\mathbf{A}(\mathbf{x}) = \sum_{a \in \mathbf{A}} f(\mathbf{x}, \mathbf{x}_{g,a}) = \sum_{a \in \mathbf{A}} \frac{1}{(\sqrt{2\pi})^k} \frac{1}{\sigma^k} e^{-\|\mathbf{x}-\mathbf{x}_{g,a}\|^2/2\sigma^2}, k \in \{1,2,3\} \tag{6}$$

where, $\mathbf{A}$ is a set of all AE events that occurred in the measuring time and space range, $\mathbf{x}_{g,a}$ is the estimated location of event a, and other parameters are defined same as before. The integral of $p_\mathbf{A}(\mathbf{x})$ over the whole space equals the number of AE events in the set $\mathbf{A}$.

Fig. 2 illustrates the whole approach which uses the estimated source location and error properties to calculate the pdAE field which shows the probability of the locations of AE events.
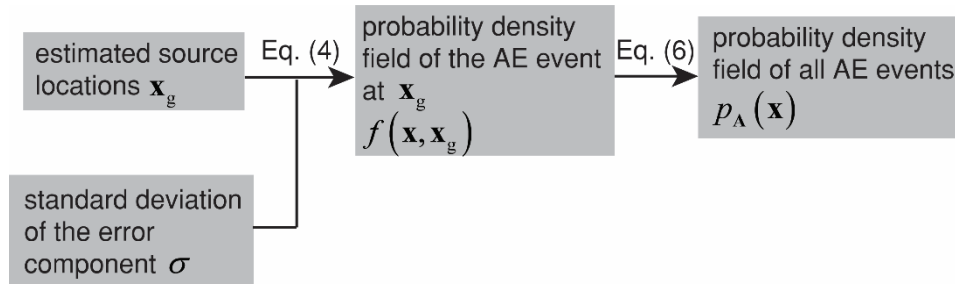

Fig. 2: Derivation of probability density field of AE events.

3. Experiments

3.1 Test setup

The dimensions of the reinforced concrete slab specimens are 5000 mm × 2500 mm × 300 mm (Fig. 3). The concrete class is C35. The specimen is reinforced with ribbed bars. The reinforcement mesh is of 21Ø20 mm bars with a spacing of 125 mm in the longitudinal direction and 41Ø10 mm bars with a spacing of 125 mm in the transverse direction. The concrete cover is 25 mm.
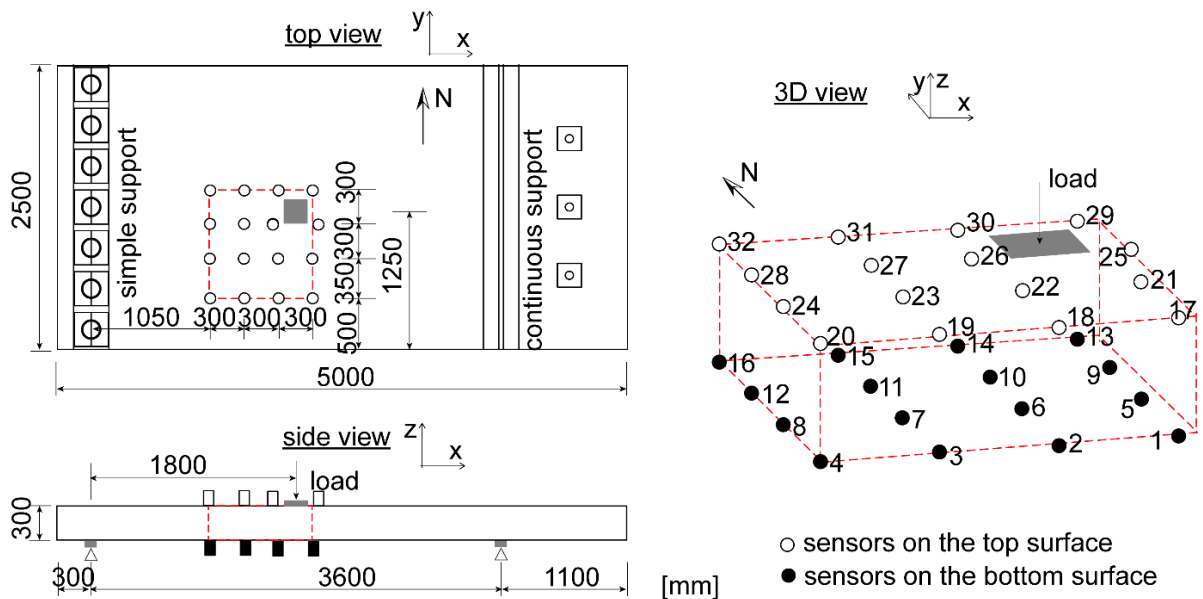

Fig. 3: A sketch of slab configuration including slab dimension, AE sensor layout and locations of supports and load.

The slab was supported at one end by seven separate bearings forming a simple support, and at the other by a line support with a cantilever of 1.1 m. At the end of the cantilever, a downward force of 45 kN was applied by three prestressing bars (15 kN each), to simulate the clamping moment at a continuous support. Fig. 4a shows a photo of the test setup.

The slab was loaded by a single point load, with shear span of 1800 mm. The load was applied through the hydraulic jack in a displacement-controlled manner. The loading speed was 0.04 mm/s. Fig. 4b shows the loading history. The loading protocol can be divided into two parts. The first part was carried out as a proof load test. The detailed considerations have been reported by Zarate

Garnica [9]. The second part included load cycles of higher load level. In the end, the slab was loaded to failure (at 1125 kN). For every load level, three or four load cycles were applied. When reading a higher load level, the load was increased in a step of around 50 kN to enable a good control of load execution. At every load step, the load was hold for a while to mark the crack patterns on the structural surface and take photos for digital image correlation (DIC).
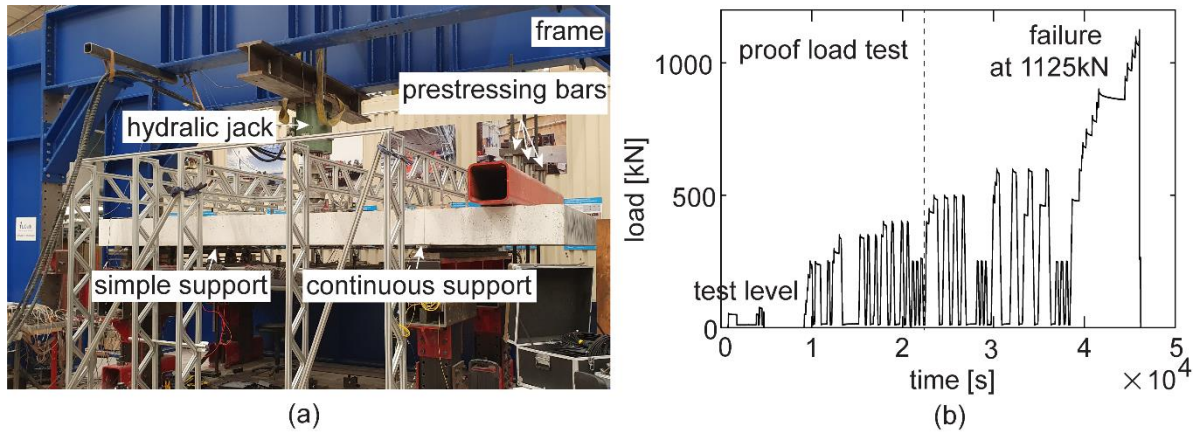

Fig. 4: (a) Photo of test setup including frame, supports and hydraulic jack, (b) loading history.

3.2 AE monitoring

AE sensors of type R6I from MISTRAS [10] were used. The central frequency is 60 kHz. The sensor was fixed to the specimen by a steel holder. Grease-like material from MOLYKOTE [11] was used as couplant between the sensor surface and structural surface. Sensors were installed both on the top and bottom surfaces. The sensor spacing in each direction was around 0.3 m, with minimum 0.25 m and maximum 0.425 m. Fig. 3 shows the sensor layout.

After installation, pencil lead break tests were carried out next to the sensor to prove sufficient coupling effect. Pencil lead with grade 2H and diameter 0.3 mm was used. The coupling was verified when the peak amplitude of the received signal was higher than 90 dB.

The data acquisition system is a 32-channel MISTRAS Express-8 system. The threshold for recording a signal was set to 45 dB. The arrival time of each signal was also automatically picked using a threshold of 45 dB.

Before loading, a preliminary measurement on wave speed was carried out (the detailed setups can refer to the thesis [12]). One sensor emitted the signal and the others received. Based on the wave travel time and distance, we estimated the wave speed. The wave speed was around 3000 m/s on the top surface and around 4000 m/s on the bottom surface. A lower wave speed on the top surface could be due to a rougher surface or more air bubble near the top. In any case, the layer that was influenced was shallow compared to the whole slab height. Therefore, we did not consider the effect of variant wave speed and used the wave speed on the bottom surface (4000 m/s) for the whole slab.

With the information of wave speed, sensor locations and arrival times of the signals, we estimated the source locations in 3D using grid search method. The grid point had a spacing of 10 mm in each direction. Source localization results outside the sensor enclosed zone were not accurate, thus were not considered.

Based on the estimated source locations, we calculated the pdAE field. The error property standard deviation of error component σ was taken as 55 mm, considering the influence from arrival time picking error and presence of cracks between source and receiver. This value is from simulated tests that have similar setups as the experiments in this paper [4].

3.3 Other measurements

Except for AE monitoring, other sensors were applied during the load testing, including laser distance finder, linear variable differential transformer (LVDT) and digital image correlation (DIC). Among them, DIC measurement is used in this paper. Photos of the bottom surface and the south surface were taken when reaching every load step. Compared to the reference (the photo that was taken before loading), the displacement field of the photo at every load level was calculated. The displacement field was then converted into the principle strain distribution, which showed the crack patterns on the bottom and side surfaces. Detailed setups can be found in the measurement report [9].

4.   Results

4.1 Crack patterns on the structural surface from DIC

Fig. 5a shows the crack patterns right before failure (at 1100 kN) on the bottom and south surface obtained from DIC. The zone near loading plate was more damaged. Due to out-of-plane displacement, it is hard to estimate the crack width from DIC. The slab failed in punching at 1125 kN with a large crack opened in the north part of the bottom surface (Fig. 5b).
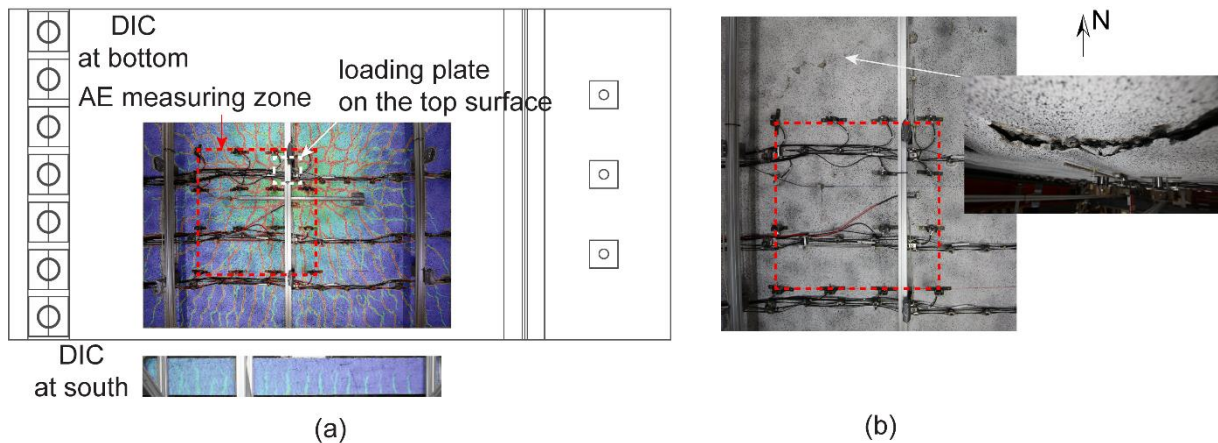

Fig. 5: Crack patterns on the bottom and the south surfaces (a) from DIC right before failure, (b) from observation after failure.

4.2 Internal crack patterns from traditional localization method

Fig. 6 shows the located AE events from the start of test to the structural failure (AE events during unloading are not included). Plot a shows the estimated locations in 3D, plot b and c respectively show the AE events in the upper and lower part of the slab in x-z plane. The estimated source locations are scattered and hard to determine the crack pattern. This is due to the larger source localization error, especially in our case when multiple cracks present between two sensors (referred to the crack patterns in Fig. 5a.
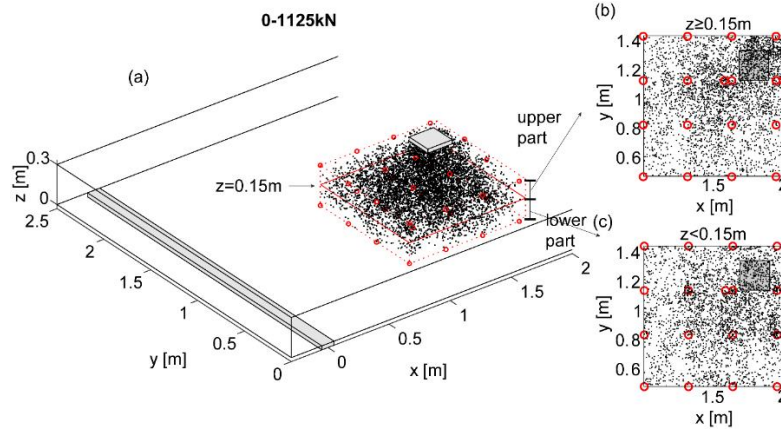
Fig. 6: Estimated source locations from grid search method until failure (0-1125 kN) excluding AE events during unloading: (a) in 3D volume, (b) in the upper part ($z \geq 0.15$ m) in *x-y* plane and (c) in the lower part ($z < 0.15$ m) in *x-y* plane.

4.3 Internal crack patterns from pdAE field method

Based on the estimated source location, we calculated the phAE field in 3D. Fig. 7 shows the sectional results from the start of test to the failure (excluding AE events during unloading). Comparing the pdAE fields at the two horizontal sections at different heights (Fig. 7b and Fig. 7c), we find that the cracks tended to concentrate to the loading plate when approaching the top section (where was the compressive zone). Comparing the pdAE fields at the vertical sections (Fig. 7d-f), we find that the section closer to the loading plate was more damaged.

To provide a 3D internal view, we plot the results in voxels (Fig. 7g). The voxel size is 20 mm × 20 mm × 20 mm. The voxel is plotted in different colours according to the pdAE value. The voxel is plotted in red, where the pdAE is over the ½ of the max pdAE. The voxel is plotted in yellow, where the pdAE is in range (¼, ½) of the max pdAE. The voxel is not plotted, where the pdAE is below ¼ of the max pdAE. The max pdAE in the detection zone is found to be 71827 m^{-3}. In 3D, the pdAE field shows a shape of punching cone under the loading plate. This meets our expectation for a punching failure. The pdAE field can more clearly detect the internal crack patterns compared to the estimated source locations using traditional method (Fig. 6).
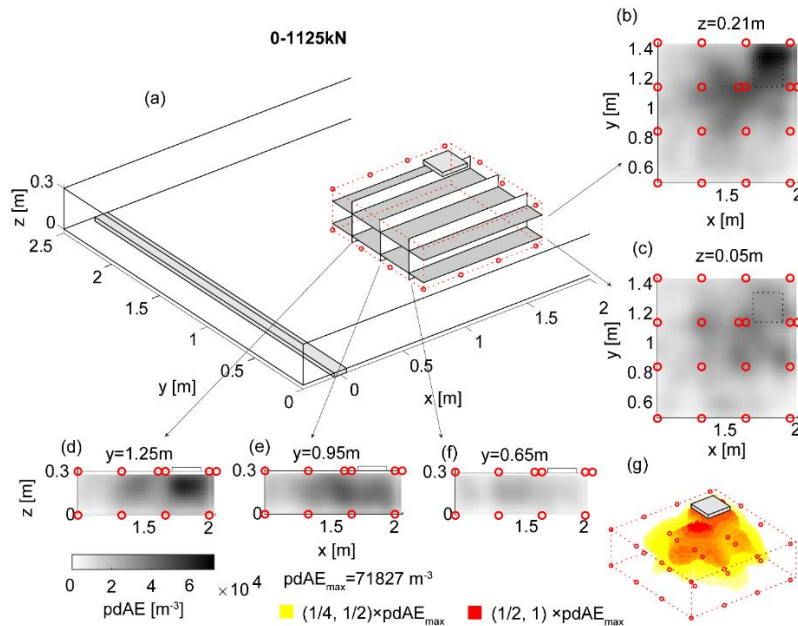

Fig. 7: The pdAE field of AE events until failure (0-1125 kN) excluding those during unloading: (a) locations of the selected cross sections, (b) sectional field at *z*=0.21 m, (c) sectional field at *z*=0.05 m, (d) sectional field at *y*=1.25 m, (e) sectional field at *y*=0.95 m, (f) sectional field at *y*=0.65 m and (g) voxel plot in 3D.

When new AE events occurred (excluding those during unloading), the pdAE fields from the new events were added up to the existing field. We updated the pdAE field every load step. Fig. 8 exemplifies the pdAE fields until 400 kN, 750 kN, 950 kN and 1050 kN. At 400 kN (plot a), AE events most occurred under the loading plate where the bending moment was the largest. This indicates the flexural cracking. At 750 kN (plot b), the internal cracks already formed a shape of punching cone under the loading plate, which could be a foreseen of punching failure. With further loading (until 950 kN and 1050 kN), the number of AE events increased, indicating further opening of the internal cracks that ended up as a punching cone. The results show that the pdAE field is able to indicate the punching failure before it occurs.
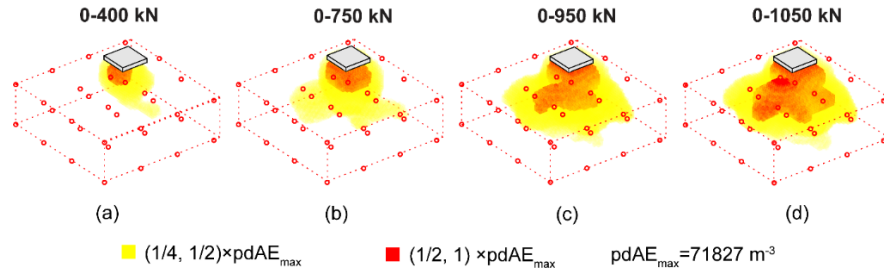

Fig. 8: The pdAE field in 3D voxels (a) until 400 kN, (b) until 750 kN, (c) until 950 kN and (d) until 1050 kN (all without AE events during unloading).

Another favourable feature of pdAE field to indicate structural failure is that the pdAE field can be computed time-efficiently. In this test, it cost less than 0.12 s to update the pdAE field when one new AE event occurred. This time was much less than other probabilistic methods in literatures (which was around 50 s) [13,14]. Moreover, updating a set of AE events together used less time than one event by another. For example, updating a set of 347 events used around 9 s, resulting in an average of 0.03 s for one event. We used Matlab to calculate, and the computational time can be improved by using faster programming language like C/C++. The effective computation of the pdAE field makes the method suitable for real-time monitoring during load testing.

5. Discussions

The above demonstration shows the benefits of using pdAE field in identifying internal damages. Firstly, compared to DIC, the pdAE field method can indicate the internal damages which are important for structural assessment. In the presented test, we detected the formation of punching cone inside the structure before the failure occurred.

Secondly, compared to traditional source localization methods, the pdAE field method can more clearly distinguish the crack patterns, by considering the source localization error in a probabilistic manner.

Thirdly, compared to other probabilistic methods in literatures [13,14], the pdAE field method significantly reduces the computational time and is suitable for a real-time monitoring.

Moreover, we found a higher pdAE in the region that was expected to be more damaged (Fig. 7 and Fig. 8). However, we were not able to build the relationship between pdAE and crack width in the presented test, since we lacked an accurate measurement of the crack width. DIC cannot measure the crack width without compensating the out-of-plane displacement. But in a previous demonstration in beams, a close relationship between pdAE and crack width has been found [4].

To implement the pdAE field method in other tests, some remarks are addressed.
- To estimate the source location, one can use any localization method. But the resultant error property needs to be adjusted correspondingly. One can use the simulations proposed in the previous paper [4] to evaluate the error property.
- For the studies that only require the crack patterns, one can directly use the source localization error property σ in range of 39-55 mm [4], without running the simulations.

- For a real-time monitoring, the pdAE field can be updated every AE event, every load step or every time interval like 60 s, depending on the users' need. The total delay of the pdAE field is the sum of time interval and calculation time.

6.   Conclusions

This paper evaluated the performance of the pdAE field method in identifying the internal damages in reinforced concrete slabs. The pdAE field estimates the probability of the locations of AE events, considering the inevitable source localization errors. We demonstrated the method in the load testing of a reinforced concrete slab. A 3D pdAE field was computed and updated with increasing load. The results showed a clearer internal crack patterns compared to the traditional localization process. Moreover, the calculation of pdAE was computationally efficient, which served for a real-time monitoring. With these benefits, the pdAE field method was able to indicate the punching failure of the slab before it occurred.

7.   References

[1]   T. Kundu, Acoustic source localization, Ultrasonics 54(1) (2014) 25-38.

[2]   M. Ohtsu, Recommendation of RILEM TC 212-ACD: Acoustic emission and related NDE techniques for crack detection and damage evaluation in concrete: Test method for classification of active cracks in concrete structures by acoustic emission, Materials and Structures 43(9) (2010) 1187-1189.

[3]   M. Ohtsu, M. Uchida, T. Okamoto, S. Yuyama, Damage assessment of reinforced concrete beams qualified by acoustic emission, ACI Structural Journal 99(4) (2002) 411-417.

[4]   F. Zhang, Y. Yang, M. Naaktgeboren, M.A.N. Hendriks, Probability density field of acoustic emission events: Damage identification in concrete structures, Construction and Building Materials 327 (2022) 126984.

[5]   C. Grosse, M. Ohtsu, Acoustic emission testing: Basics for Research-Applications in Civil Engineering, 2008.

[6]   S. Gollob, Source localization of acoustic emissions using multi-segment paths based on a heterogeneous velocity model in structural concrete, ETH Zürich, 2017.

[7]   F. Zhang, L. Pahlavan, Y. Yang, Evaluation of acoustic emission source localization accuracy in concrete structures, Structural Health Monitoring 19(6) (2020) 2063-2074.

[8]   M.L.L. Abell, J.P. Braselton, J.A. Rafter, J.A. Rafter, Statistics with Mathematica, Elsevier Science1999.

[9]   G. Zarate Garnica, Measurement report of reinforced concrete slabs, Stevin Report, Delft University of Technology, Delft, the Netherlands, 2021.

[10]   MISTRAS, R6I-AST Sensor, Product Data Sheet, MISTRAS Group Inc., Princeton Junction, NJ 08550, 2008.

[11]   MOLYKOTE, MOLYKOTE 4 Electrical Insulating Compound, Product Data Sheet, DuPont de Nemours, Inc., 2018.

[12]   F. Zhang, Acoustic emission-based indicators of shear failure of reinforced concrete structures without shear reinforcement, Civil Engineering and Geosciences, Delft University of Technology, Delft, the Netherlands, to be published.

[13]   T. Schumacher, D. Straub, C. Higgins, Toward a probabilistic acoustic emission source location algorithm: A Bayesian approach, Journal of Sound and Vibration 331(19) (2012) 4233-4245.

[14]   M.R. Jones, T.J. Rogers, K. Worden, E.J. Cross, A Bayesian methodology for localising acoustic emission sources in complex structures, Mechanical Systems and Signal Processing 163 (2022) 108143.